ARTICLE

Adsorptive Avidity of Prussian blue Polypyrrole Nanocomposite for Elimination of Water Contaminants: a Case study of Malachite Green and Isoniazid

Tabee Jan,[a] Shabnam Raheem,[a] Aamir Hanif,[b] Gaulthier Rydzek,[c] G.M. Peerzada,[a] Katsuhiko Ariga,[d,e] Jin Shang,[f] Masood Ahmad Rizvi.[a*]

Supplementary Data:

Figure S1: TGA/DTA analysis of PB and PPY

Figure S2: XRD patterns of PPY, PB and PPY/PB nanocomposite powders

Figure S3. Elemental mapping images of C,N and Fe of PB

Figure S4. Elemental mapping images of C,N and Fe of PPY/PB nanocomposite

Figure S5: Effect of the initial adsorbate concentration and adsorbent dose on the adsorption capacity of PPY/PB nanocomposite

Figure S6: Non-linear fitted curves of isotherm models

Figure S7: Effect of temperature on the removal efficiency of M.G. and INH

Figure S8: Adsorption studies of M.G. and INH in real water samples and assessment of the reusability of the PPY/PB nanocomposite

Figure S9. Stability of PPY/PB nanocomposite under harsh conditions (pH=7 and 9) (A) FTIR spectra and (B)Tauc plot for band gap(E_g) calculation through Diffuse Reflectance Spectroscopy(DRS)

Figure S10. Effect on removal efficiency in a ternary mixture of M.G. INH, and 4 NP using PPY/PB under optimized conditions.

Figure S11: UV-Vis analysis of 4-NP in the presence of PPY/PB catalyst under visible light and dark conditions

Figure S12: Photograph showing the color change indicative of the conversion of 4-NP to 4-AP in the presence of PPY/PB catalyst

Figure S13: Pseudo first order kinetic plots and evolution of the conversion rate of 4-NP to 4-AP at different PPY/PB dosages.

Figure S14: UV-Vis analysis of 4-NP at constant concentration of 4-NP and catalyst by varying [$NaBH_4$]. Evolution of their Pseudo-first order kinetic plots and comparison of their apparent rate constants

Figure S15: **:** UV-Vis analysis of 4-NP in the presence of fixed amount of $NaBH_4$ and catalyst at different [4-NP]. Evolution of their Pseudo-first order kinetic plots and comparison of their apparent rate constants

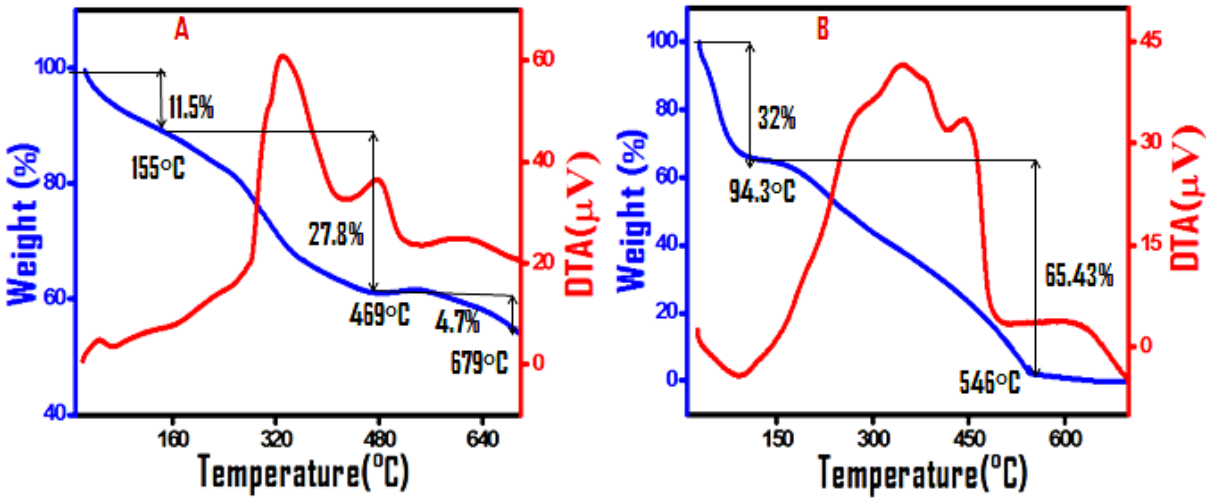

Figure S1. TGA/DTA analysis of (A) PB nanoparticles depicting three loss steps, and (B) PPY showing two loss steps.

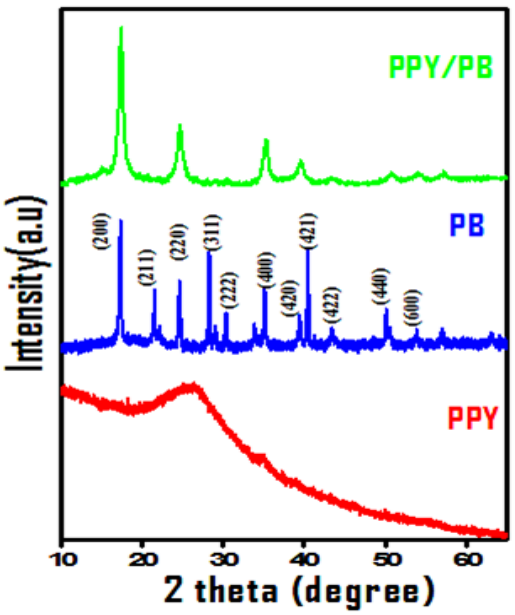

Figure S2. XRD patterns of PPY, PB and of the PPY/PB nanocomposite

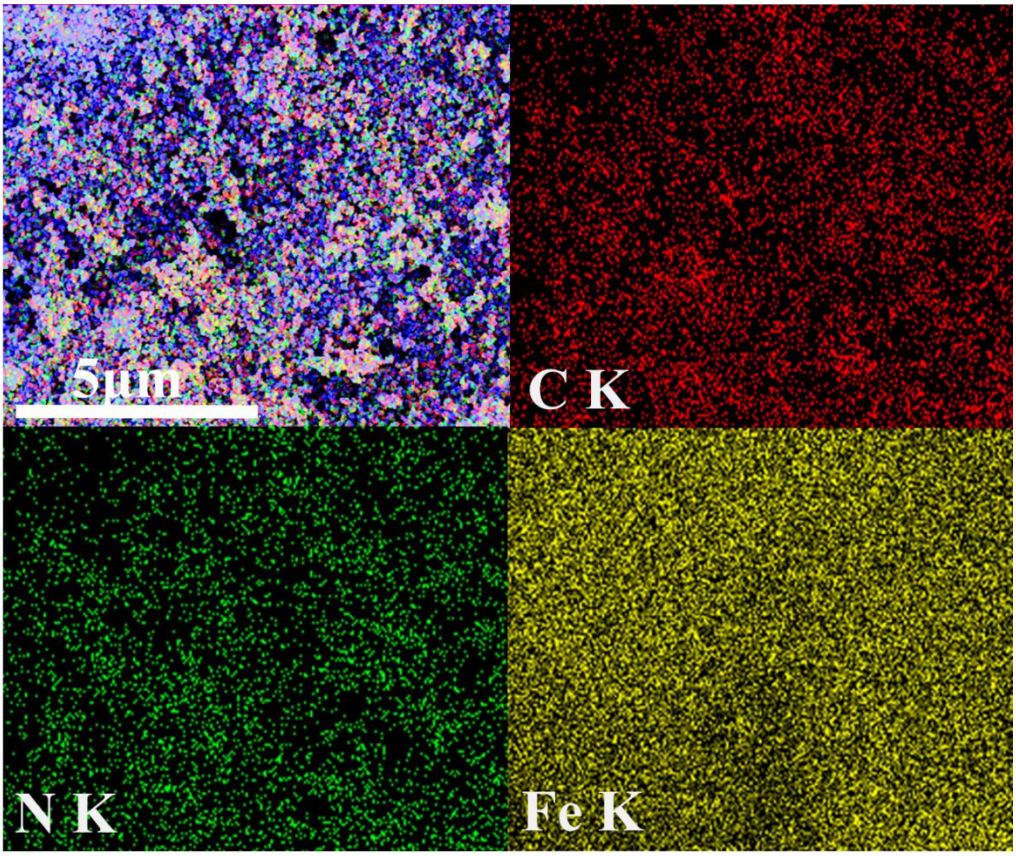

Figure S3. Elemental mapping images of C,N and Fe of PB

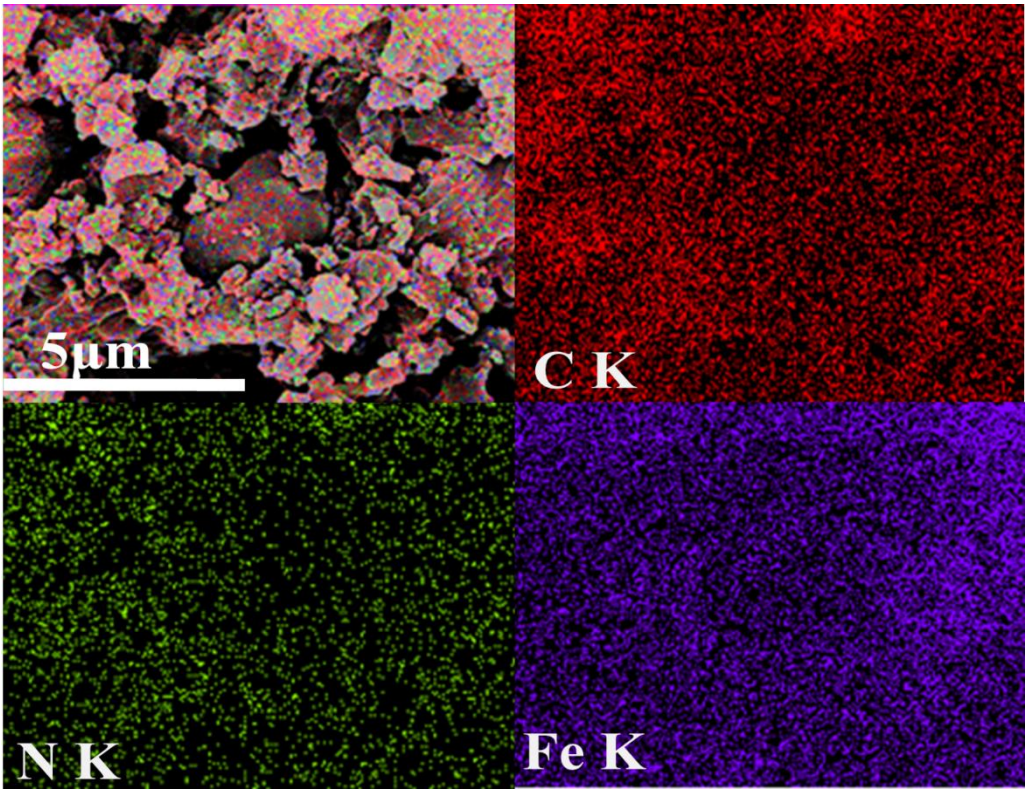

Figure S4. Elemental mapping images of C,N and Fe of PPY/PB nanocomposite

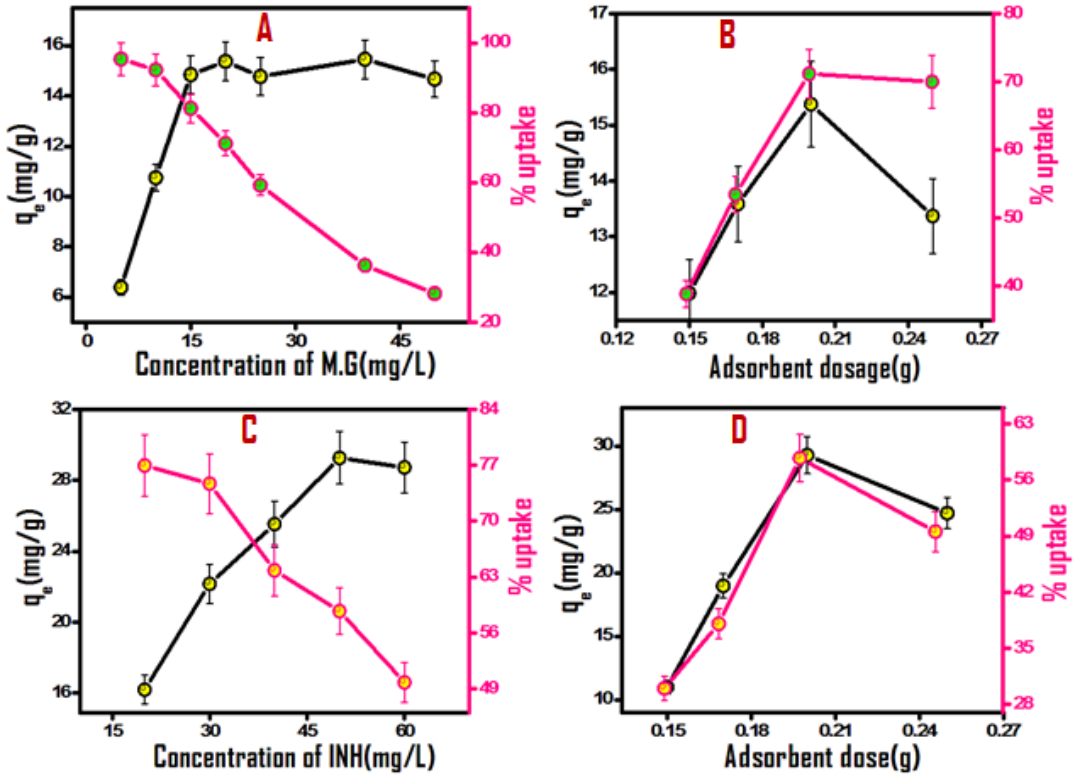

Figure S5. Effect of the initial adsorbate concentration on the adsorption capacity of PPY/PB towards (A) M.G and (C) INH. Concentration conditions of Ci= 5-30 mg/L (M.G.) and 10-60 mg/L (INH) were used at T= 298 K, pH 7. Contact times of 400 min (M.G.) and 360 min (INH) were used with V=200 mL, and a PPY/PB dose of 1mg/mL. Adsorbent dose effect on the removal efficiency of (B) M.G and (D) INH under conditions of Ci= 20mg/L (M.G) and 50 mg/L (INH) after 400 min (M.G.) and 360 min (INH) of contact time. The total volume was 200 mL with a PPY/PB dose of 150-250mg

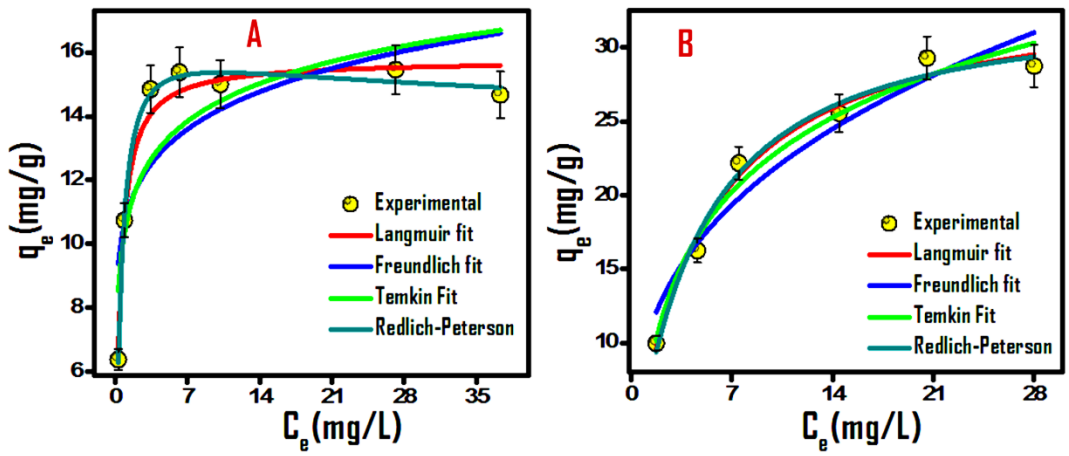

Figure S6 Non-linear fitted curves of isotherm models for (A) M.G and (B) INH under conditions of Ci=5-40 mg/L (M.G.) and 10-60 mg/L (INH). Experiments were carried out at pH7, T=298K, using a 200 mL of a 1 mg/mL PPY/PB dispersion with a contact time of 400 min (M.G.) and 360 min (INH).

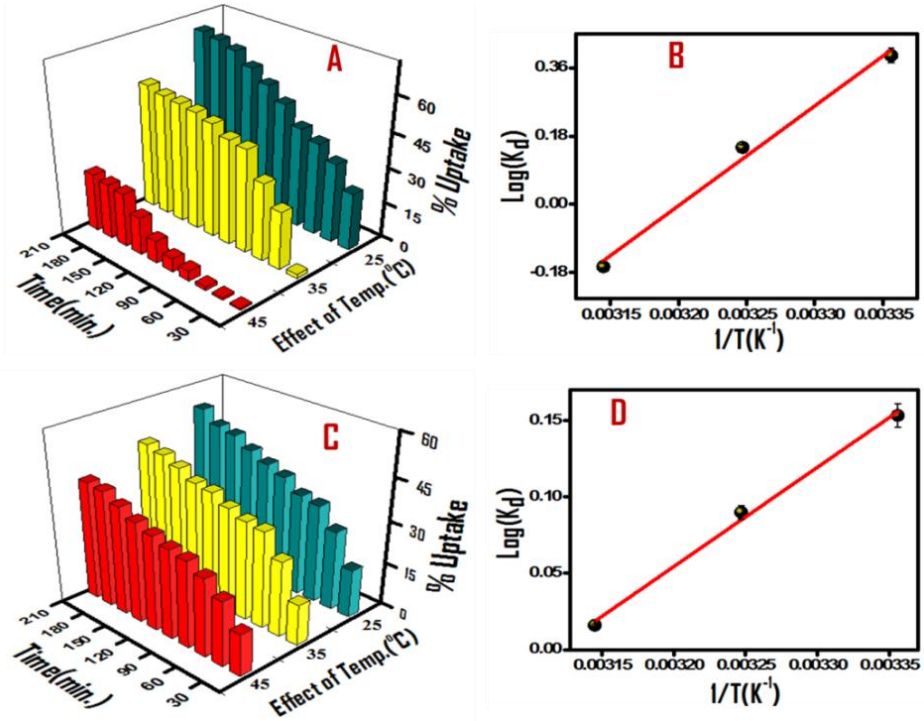

Figure S7. Effect of the temperature on the removal efficiency of (A) M.G. and (C) INH under conditions of Ci=20 mg/L (M.G) and 50 mg/L(INH) at pH 7 and T=298-318K. Experiments were carried out using 200 mL of a 1 mg/mL PPY/PB dispersion with a contact time of 20 to 200 min.Van't Hoff plots for calculation of thermodynamic parameters regarding the sorption of (B) M.G. and (D) INH.

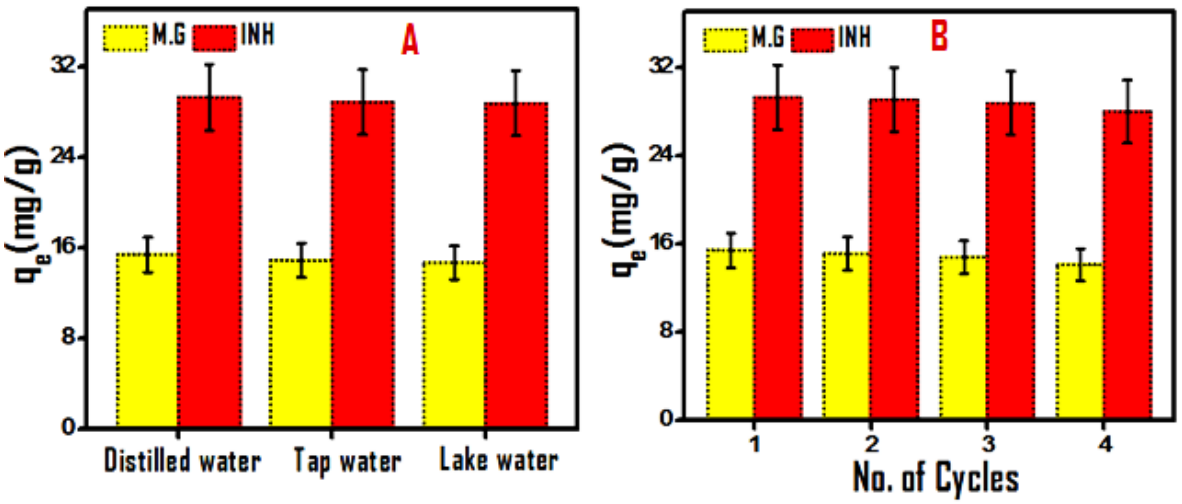

Figure S8. (A) Adsorption of M.G and INH onto the PPY/PB nanocomposite in real water samples. (B) Reusability of PPY/PB nanocomposite after M.G. and INH adsorption

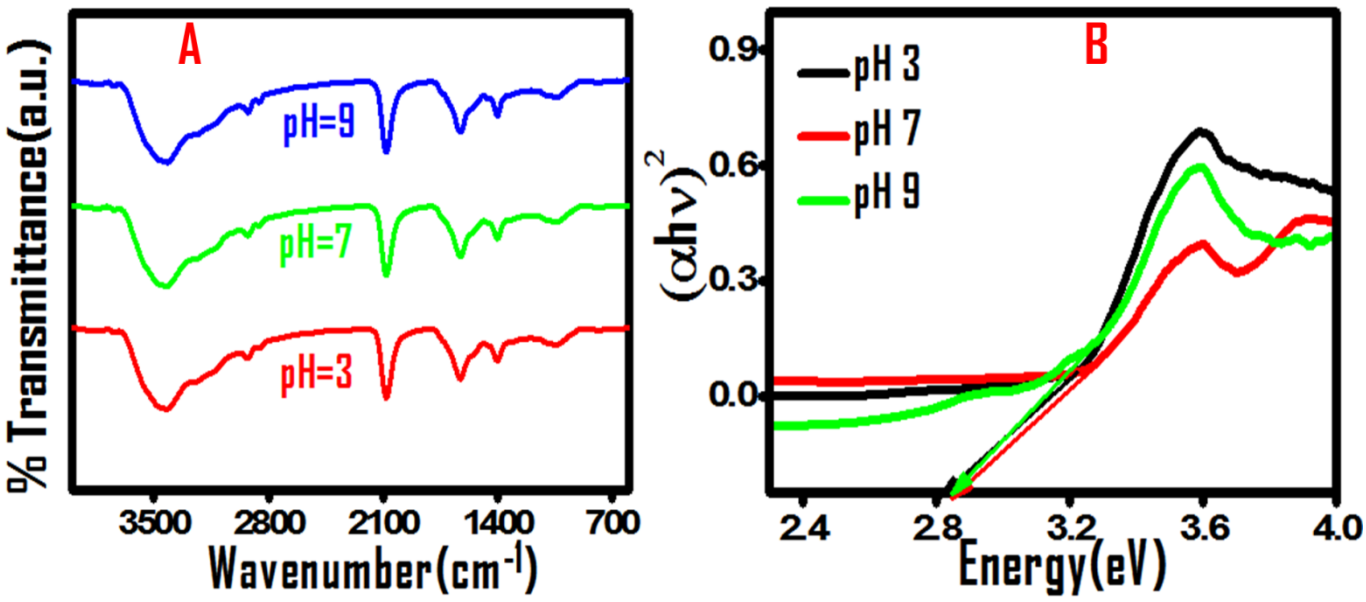

Figure S9. Stability of PPY/PB nanocomposite under harsh conditions (pH=3 and 9) (A) FTIR spectra and (B)Tauc plot for band gap(E_g) calculation through Diffuse Reflectance Spectroscopy(DRS)

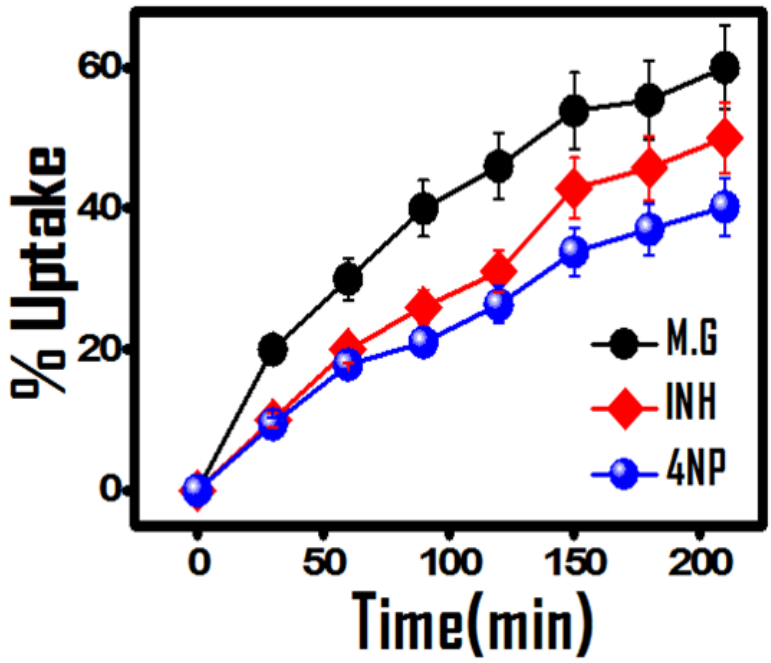

Figure S10. Effect on removal efficiency in a ternary mixture of M.G. INH, and 4 NP using PPY/PB under optimized conditions.

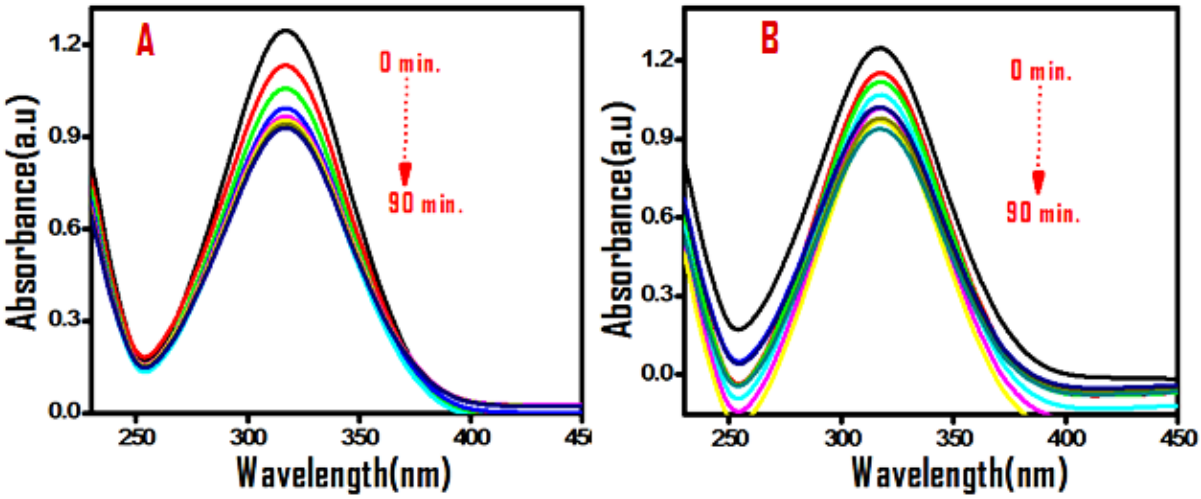

Figure S11. Time dependent UV-Vis analysis of 4-NP in the presence of PPY/PB catalyst under (A) visible light irradiation and (B) dark conditions.

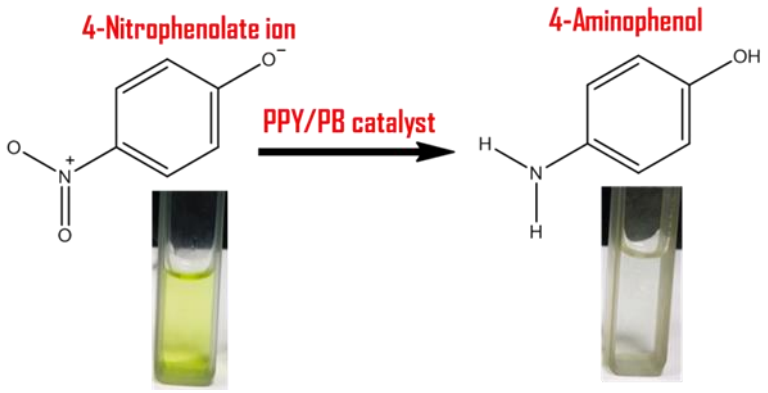

Figure S12. Color change indicating the conversion of 4-NP to 4-AP in the presence of PPY/PB catalyst

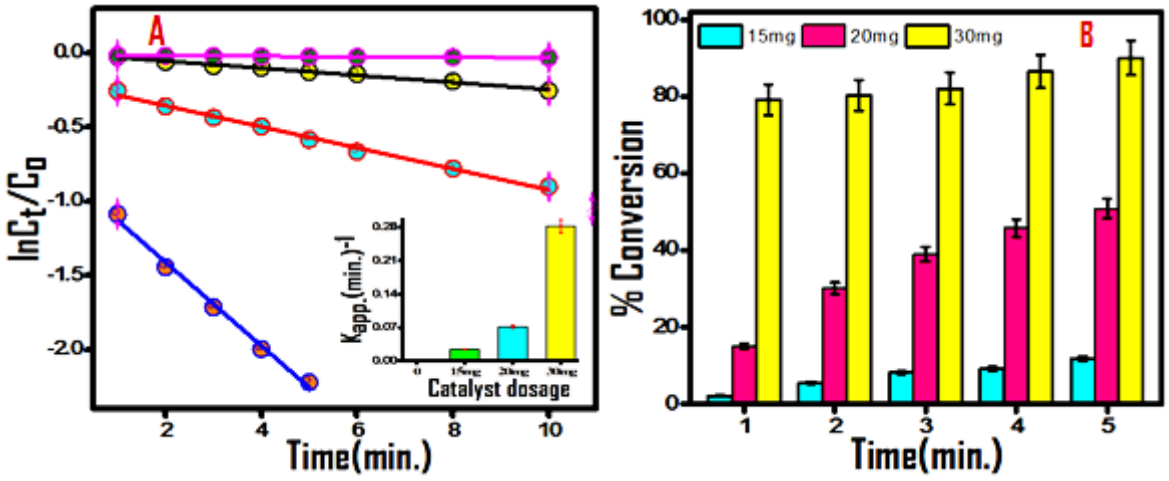

Figure S13 (A) Pseudo first order kinetic plots and (B) conversion rate of 4-NP (0.1mM) to 4-AP at different time intervals in the presence of different dosage of PPY/PB catalyst .

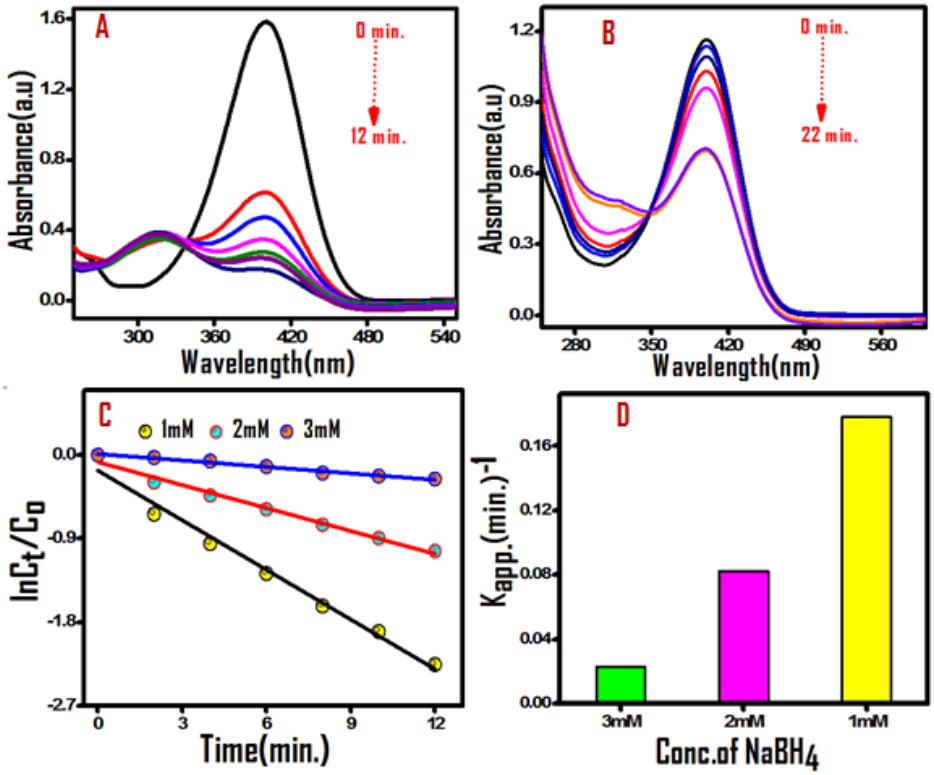

Figure S14. Time dependent UV-Vis analysis of 4-NP in the presence of fixed amount of 4-NP and PPY/PB catalyst (0.1 mM, 20 mg) at different concentrations of $NaBH_4$: (A)1 mM and (B) 3 mM). (C) Pseudo-first order kinetic plot and (D) comparison of apparent rate constants obtained from the slope of pseudo-first order fit at different $NaBH_4$ concentrations.

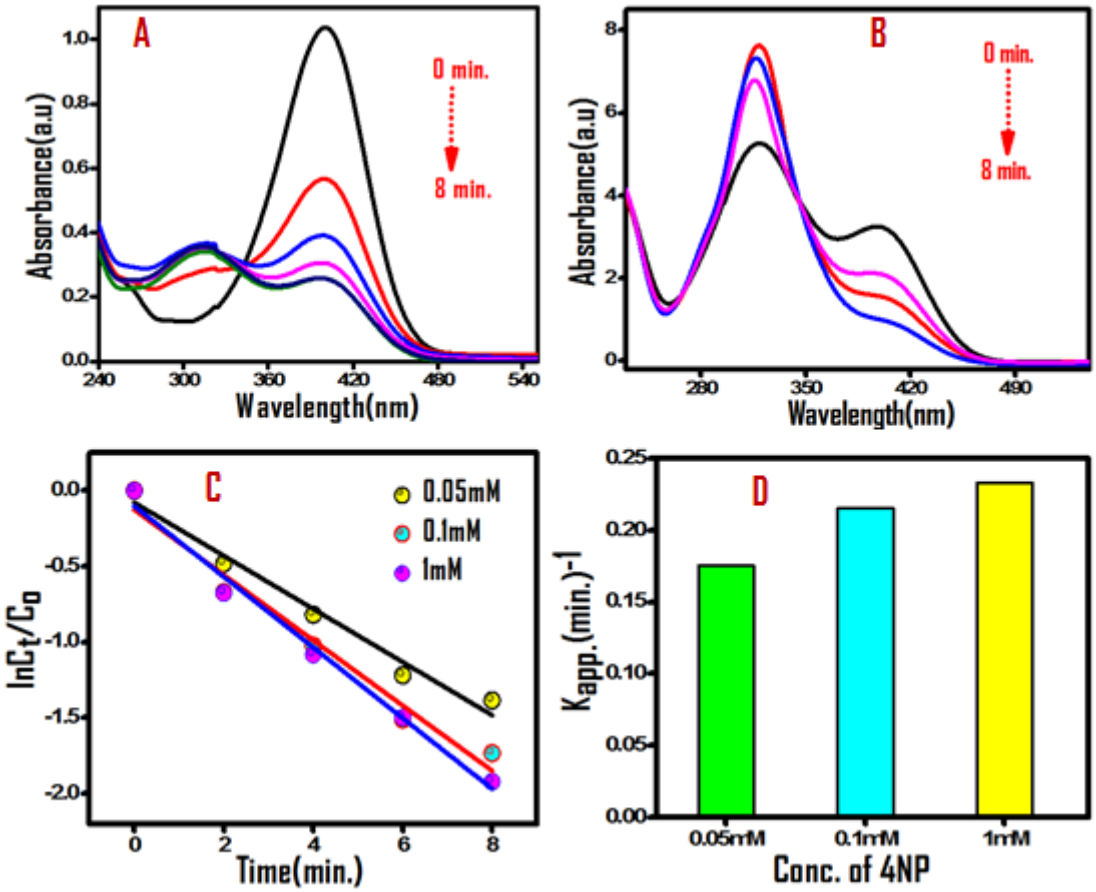

Figure S15. UV-Vis analysis of 4-NP solutions in the presence of fixed dosage of $NaBH_4$ and PPY/PB catalyst (1 mM, 20 mg) and with varying concentrations of 4-NP: (A) 0.05 mM and (B)1 mM. (C) Their kinetic plots and (D) comparison of their apparent rate constants obtained from the slope of pseudo-first order fit at different 4-NP concentrations .